Available online at www.sciencedirect.com
SCIENCE DIRECT®
ELSEVIER
International Journal of Solids and Structures xxx (2005) xxx–xxx
INTERNATIONAL JOURNAL OF SOLIDS and STRUCTURES
www.elsevier.com/locate/ijsolstr

Generation of artificial earthquakes via the wavelet transform

Luis E. Suárez *, Luis A. Montejo

Department of Civil Engineering University of de Puerto Rico Mayagüez 00681-9041 Puerto Rico

Received 9 January 2005

Abstract

A wavelet-based procedure is presented to generate an accelerogram whose response spectrum is compatible with a target spectrum. The acceleration time history of a recorded ground motion is decomposed into a number of component time histories. Next, each of the time histories is appropriately scaled so that its response spectrum matches a specified design spectrum at selected periods. The modified components are used to reconstruct an updated accelerogram, its spectrum is compared with the target spectrum and the process is repeated until a reasonable match is obtained. To achieve this goal, a new wavelet, based on the impulse response function of an underdamped oscillator is proposed. The proposed procedure is illustrated by modifying five recorded accelerograms with different characteristics so that their spectra match a seismic design spectrum prescribed in the 1997 Uniform Building Code for a seismic zone 3 and soil type S_B (rock).

Keywords: Wavelet transform; Artificial earthquakes; Spectrum compatible earthquakes

1. Introduction

The response of structures under earthquake ground motions can be calculated either using a (pseudo-acceleration) response spectrum or an acceleration time history. For design purposes, the seismic codes provide a design spectrum, i.e. a smooth response spectrum that (hopefully) takes into account every possible earthquake likely to occur in a given zone (with a certain probability of

* Corresponding author. Tel.: +1 78 78 32 40 40x3669; fax: +1 78 78 33 82 60.
E-mail address: lsuarez@uprm.edu (L.E. Suárez).

0020-7683/$ - see front matter © 2005 Elsevier Ltd. All rights reserved.
doi:10.1016/j.ijsolstr.2005.03.025

occurrence). Because special care is taken to define a reliable design spectrum, and since the response spectrum method is a simple and well-established procedure, it is the most common approach to perform linear analysis of buildings and other conventional structures. However, the seismic analysis of many critical structures (such as power plants, dams, tall buildings, cable-stayed bridges, etc) is usually done using a step-by-step time analysis. Moreover, the application of the response spectrum method to nonlinear analysis is not straightforward. Thus, in many cases a nonlinear dynamic analysis is done, which requires an accelerogram representative of an earthquake expected at the site. Except for very few regions of the world where a set of recorded accelerograms are available, artificial earthquakes are used for the dynamic analysis. These earthquakes are defined by accelerograms that are "consistent" with a design spectrum, i.e. they are such that if their response spectra are calculated, they will be approximately equal to a prescribed or target spectrum. The artificial accelerograms can be generated from the superposition of sine waves with random phases and the resulting amplitude modulated by a smooth function to account for the transient character of the seismic motions (Vanmarcke and Gasparini, 1976). An alternative method is to modify appropriately the records of historic earthquakes so that their spectra match the design spectrum. This is the approach followed in this paper.

2. The wavelet transform

The wavelet transform is a two-parameter transform: for a time signal $f(t)$, the two transformed domains are time p (also referred to as position) and scale s. The scale s can be approximately related to frequency: it is inversely proportional to a frequency that depends on the type of wavelet used, as it will become apparent later. In simple terms, wavelets are localized waves, i.e. signals with a zero average value that rapidly drop to zero after a few oscillations. To apply the wavelet transform one must select a suitable wavelet $\psi(t)$ from those available in the literature (Misiti et al., 2000). This function is usually referred to as the "mother wavelet". To perform the transform, the mother wavelet is scaled by a real constant $s > 0$, (the scale) and shifted by a real parameter p (the position):

$$\psi_{s,p}(t) = \frac{1}{\sqrt{s}}\psi\left(\frac{t-p}{s}\right) \tag{1}$$

The continuous wavelet transform of a time signal can now be defined as the sum over all times of the signal multiplied by the scaled and shifted version of the original (mother) wavelet:

$$C(s,p) = \frac{1}{s}\int_{-\infty}^{\infty} f(t)\psi\left(\frac{t-p}{s}\right)\mathrm{d}t = \int_{-\infty}^{\infty} f(t)\psi_{s,p}(t)\mathrm{d}t \tag{2}$$

Although for the present purpose we will use to continuous version, it should be pointed out that most of the applications of wavelets deal with the discrete wavelet transform (Strang and Nguyen, 1996). In all practical applications, the coefficients $C(s,p)$ are modified somehow to achieve a given objective before they are transformed back to the original time domain. The signal $f(t)$ can be retrieved with the so-called "reconstruction formula" (Grossman and Morlet, 1984):

$$f(t) = \frac{1}{K_\psi}\int_{s=0}^{\infty}\int_{p=-\infty}^{\infty} C(s,p)\psi_{s,p}(t)\mathrm{d}p\frac{\mathrm{d}s}{s^2} \tag{3}$$

The constant K_ψ depends on the mother wavelet selected, and is defined as (Mallat, 1999):

$$K_\psi = \int_0^{\infty}\frac{|\psi(\omega)|^2}{\omega}\mathrm{d}\omega < \infty \tag{4}$$

3. The new impulse response wavelet

The selection of the proper wavelet for a given application is crucial for the successful implementation of the wavelet transform. For the generation of artificial earthquakes we tried several candidates. With the exception of the Littlewood–Paley wavelet used by Basu and Gupta (1998), all the other wavelets were unable to achieve the objective. Therefore, a new wavelet, based on the impulse response function of an underdamped oscillator, was proposed. The mother wavelet has the following form:

$$\psi(t) = \mathrm{e}^{-\zeta\Omega|t|}\sin\Omega t \tag{5}$$

where ζ and Ω are two parameters that govern the decrement and the time variation of the wavelet. They can be identified with the damping ratio and natural frequency of a single degree of freedom oscillator. The wavelet must be defined for $t < 0$ and it should go to zero as $t \to \infty$ and as $t \to -\infty$. Therefore, the absolute value of t is used in the exponential. This, in turn, leads to an anti-symmetric wavelet as it is shown in Fig. 1.

The Fourier transform $\psi(\omega)$ of the wavelet function $\psi(t)$ proposed in Eq. (5) is defined by:

$$\Psi(\omega) = F[\psi(t)] = \int_{-\infty}^{\infty}\psi(t)\mathrm{e}^{-\mathrm{i}\omega t}\mathrm{d}t = \int_{-\infty}^{\infty}\mathrm{e}^{-\zeta\Omega|t|}\sin(\Omega t)\mathrm{e}^{-\mathrm{i}\omega t}\mathrm{d}t \tag{6}$$

$$\Psi(\omega) = \frac{\mathrm{i}4\zeta\omega\Omega^2}{\omega^4 + 2(\zeta^2-1)\omega^2\Omega^2 + (\zeta^2+1)\Omega^4} \tag{7}$$

Note that the Fourier transform of the proposed wavelet is a pure imaginary function, a consequence of the anti-symmetric character of $\psi(t)$. The graph for the absolute value of the expression in Eq. (7) is shown in Fig. 2.

It can be seen from Fig. 1 that the wavelet function is limited in extent in the time domain and from the Fourier transform of the wavelet in Fig. 2 it is also bounded in the frequency domain. In other words, the wavelet and its transform are very well localized. Increasing the value for ζ gives a greater localization in the time domain, but less so in the frequency domain. A larger ζ reduces the amplitude of the peak in the Fourier transform (Montejo, 2004). The value of Ω controls the dominant frequency of the wavelet. The values of the parameters $\zeta = 0.05$ and $\Omega = \pi$ used to generate Figs. 1 and 2 are the same values that were found to be convenient for the modification of the recorded accelerograms to be explained later.

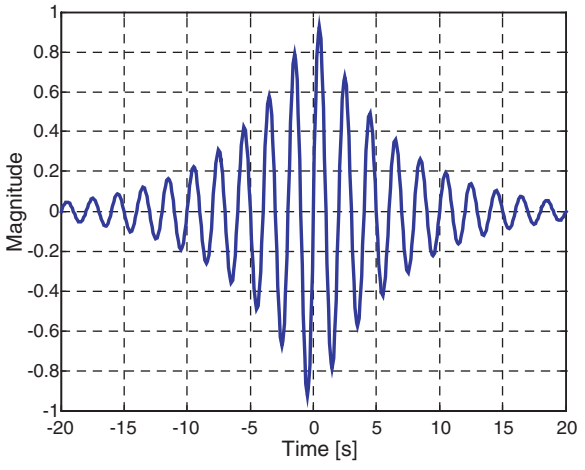

Fig. 1. The proposed Impulse Response Wavelet for $\zeta = 0.05$ and $\Omega = \pi$ rad/s.

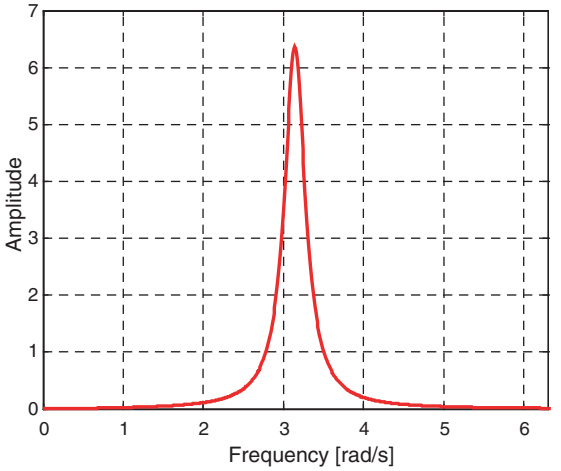

Fig. 2. The Fourier transform of the Impulse Response Wavelet for $\zeta = 0.05$ and $\Omega = \pi$ rad/s.

The reconstruction constant K_ψ for the impulse response wavelet can be obtained from Eq. (4):

$$K_\psi = 16\zeta^2\Omega^4 \int_0^\infty \frac{\omega}{[\omega^4 + 2(\zeta^2-1)\omega^2\Omega^2 + (\zeta^2+1)\Omega^4]^2}\mathrm{d}\omega$$

$$K_\psi = \frac{-4\zeta(\zeta^2-1) + \pi(\zeta^2+1)^2 + 2(\zeta^2+1)^2\tan^{-1}\left(\frac{1}{2\zeta} - \frac{\zeta}{2}\right)}{4\zeta(\zeta^2+1)^2\Omega^2} \tag{8}$$

For $\zeta = 0.05$ and $\Omega = \pi$, the value of K_ψ is 3.18.

For the discrete implementation for the wavelet transform another function, is required besides the mother wavelet. Although this work does not deal with the discrete transform, to complete the characterization of the new impulse response wavelet we will discuss this function.

Suppose that the wavelet transform $C(s,p)$ is only available for small scales, for instance $s < s_0$ and one needs to recover the function $f(t)$. In this case we need the complement somehow the information corresponding to $C(s,p)$ for $s > s_0$. To obtain this information another function $\phi(t)$, referred to as the *scaling function*, is introduced (Mallat, 1999). Substituting $\psi(t)$ by $\phi(t)$ in Eq. (2) one obtain a function $A(s_0,p)$

$$A(s_0,p) = \frac{1}{\sqrt{s_0}}\int_{-\infty}^{\infty} f(t)\phi\left(\frac{t-p}{s_0}\right)\mathrm{d}t = \int_{-\infty}^{\infty} f(t)\phi_{s_0,p}(t)\mathrm{d}t \tag{9}$$

It can then be shown (Mallat, 1999) that the inverse continuous wavelet transform in Eq. (3), i.e. the reconstruction formula, can be divided as follows

$$f(t) = \frac{1}{K_\psi}\int_0^{s_0}\left(\int_{-\infty}^{\infty} C(s,p)\psi_{s,p}(t)\mathrm{d}p\right)\frac{\mathrm{d}s}{s^2} + \frac{1}{K_\psi s_0}\int_{-\infty}^{\infty} A(s_0,p)\phi_{s_0,p}(t)\mathrm{d}p \tag{10}$$

The scaling function $\phi(t)$ is important for the numerical implementation of the discrete wavelet transform. The scaling function associated with the new impulse response wavelet can be defined by a closed form expression in the frequency domain, using a technique due to Duval-Destin et al. (1993).

The modulus of the Fourier transform of the scaling function is defined by (Duval-Destin et al., 1993; Mallat, 1999):

$$|\Theta(\omega)|^2 = \int_1^\infty \frac{|\psi(s\omega)|^2}{s}\mathrm{d}s \tag{11}$$

Applying Eq. (11) to the case of the impulse response wavelet one obtains:

$$|\Theta(\omega)| = \frac{1}{2}\sqrt{\frac{\pi\omega^4 + 2(\pi(\zeta^2-1)-2\zeta)\Omega^2\omega^2 + (-4\zeta^3+4\zeta+\pi(\zeta^2+1)^2)\Omega^4 - 2(\omega^4+2(\zeta^2-1)\Omega^2\omega^2+(\zeta^2+1)^2\Omega^4)\cot^{-1}\left(\frac{2\zeta}{\zeta^2+\frac{\omega^2}{\Omega^2}-1}\right)}{\zeta\Omega^2(\omega^4+2(\zeta^2-1)\Omega^2\omega^2+(\zeta^2+1)^2\Omega^4)}} \tag{12}$$

Figs. 3 and 4 show, respectively, the modulus of the Fourier transform of the scaling function $\phi(t)$ associated with the impulse response wavelet and the scaling function calculated using the numerical inverse Fourier Transform.

4. The proposed spectrum-matching procedure

For the application that we are interested in, the time function $f(t)$ is the ground acceleration $\ddot{X}_g(t)$ due to an earthquake. It is convenient to re-write Eq. (3) as follows:

$$\ddot{X}_g(t) = \int_{s=0}^{\infty}\left(\int_{p=-\infty}^{\infty}\frac{1}{s^2}C(s,p)\psi_{s,p}(t)\mathrm{d}p\right)\mathrm{d}s = \int_0^\infty D(s,t)\mathrm{d}s \tag{13}$$

The constant K_ψ was set equal to 1 because here we are not interested in retrieving the original time function. In other words, the function $\ddot{Y}_g(t)$ will be the accelerogram of the modified earthquake motion. The functions $D(s,t)$, which will be referred to as the "detail functions", are

$$D(s,t) = \int_{-\infty}^{\infty} C(s,p)\psi_{s,p}(t)\mathrm{d}p = \frac{1}{s^{5/2}}\int_{-\infty}^{\infty} C(s,p)\psi\left(\frac{t-p}{s}\right)\mathrm{d}p \tag{14}$$

In practice, a set of n discrete values s_j of the continuous scale s are used. Based on the values used for the discrete wavelet transform we found convenient to define them as follows

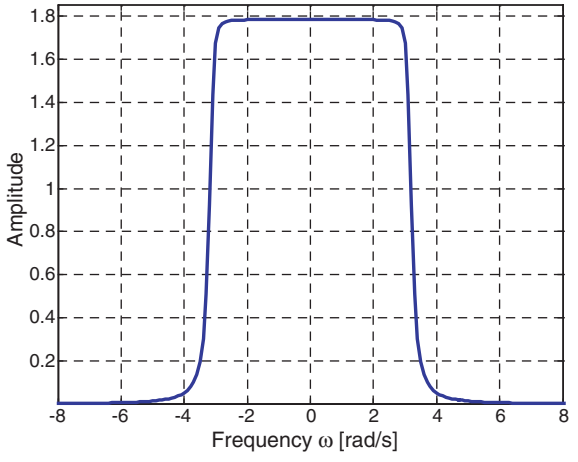

Fig. 3. The Fourier transform of the scaling function associated to the Impulse Response Wavelet for $\zeta = 0.05$ and $\Omega = \pi$ rad/s.

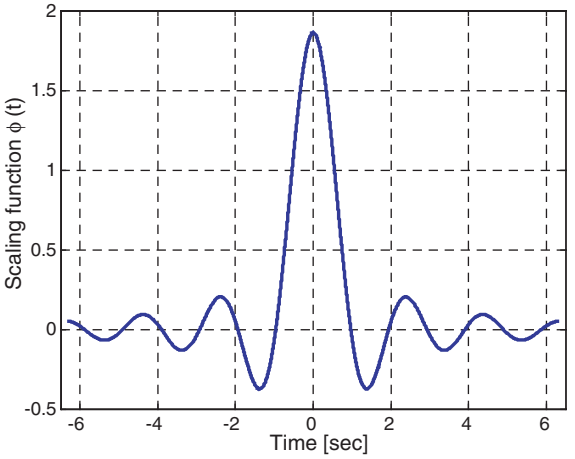

Fig. 4. Scaling function associated to the Impulse Response Wavelet for $\zeta = 0.05$ and $\Omega = \pi$ rad/s.

$$s_j = 2^{j/8}; \quad j = -(n_0 - 1), -(n_0 - 2), \ldots, -(n_0 - n) \tag{15}$$

where n is the number of discrete values of s_j and n_0 is a selected integer.

In practical applications the ground acceleration signal $\ddot{X}_g(t)$ is always sampled at equal time intervals Δt. We will assume that the accelerogram is sampled at N discrete times t_k. Since p is a time scale as well, it will also be discretized as a set of N values.

The discrete coefficients of the wavelet transform given by Eq. (2) will be calculated using the approximate expression

$$C(s_j, p_i) \simeq \frac{\Delta t}{\sqrt{s_j}} \sum_{k=1}^{N} f(t_k) \psi\left(\frac{t_k - p_i}{s_j}\right); \quad j = 1, \ldots, n; \;\; i = 1, \ldots, N \tag{16}$$

In terms of the discrete scales, the detail functions are then defined using the discrete counterpart of Eq. (14), i.e.

$$D(s_j, t_k) \simeq \frac{\Delta p}{s_j^{5/2}} \sum_{i=1}^{N} C(s_j, p_i) \psi\left(\frac{t_k - p_i}{s_j}\right); \quad j = 1, \ldots, n; \;\; k = 1, \ldots, N \tag{17}$$

Although the detail functions are not purely harmonic, they have a predominant frequency given by the dominant frequency of the dilated wavelet $\psi(\frac{t-p}{s_j})$. For the proposed impulse response wavelet, this frequency can be defined by examining the dilated wavelet obtained from Eq. (5)

$$\psi\left(\frac{t-p}{s_j}\right) = \mathrm{e}^{-\zeta\Omega\left|\frac{t-p}{s_j}\right|} \sin\left(\frac{\Omega t - p}{s_j}\right) \tag{18}$$

The predominant frequency ω_j and period T_j of each detail function are

$$\omega_j = \frac{\Omega}{s_j}; \qquad T_j = \frac{2\pi}{\Omega} s_j \tag{19}$$

The first step in the proposed procedure is the selection of the discrete scale values s_j. This must be done in such a way that the periods T_j defined in Eq. (19) reasonably span the range of periods of the seismic response spectrum which will be used as target.

Since the scale values s_j are defined as $2^{j/8}$, they are determined by the values of n_0 and n which define the index j according to Eq. (15). We found convenient to use $n_0 = 51$ and $n = 63$ for the numerical implementations. With these values, the index j goes from -50 to 12, and the scale s_j takes values from 0.0131 to 2.8284. According to Eq. (19), the frequencies ω range from 1.1107 rad/s ($T = 5.657$ s) to 238.904 rad/s ($T = 0.0263$ s).

Table 1 shows the values of the scale s_j, the predominant frequency in rad/s and Hertz, and the period for a few detail functions. Figs. 9–11 show the detail functions described in Table 1 and the corresponding Fourier transforms. The details functions were obtained from the wavelet decomposition of a particular earthquake record (the Friuli earthquake described later).

In order that those readers not familiar with the concept of response spectrum can appreciate the application of the wavelet transform presented in this article, a brief explanation is provided next. A ground response spectrum is a graphical description of the maximum response (in absolute value) of a one degree of freedom linear oscillator with a fixed damping ratio ζ, subjected to a given earthquake base acceleration, as a function of the natural period (or frequency). For design purposes, the seismic codes specify a *design* spectrum, which is a smooth curve that, in theory, is an envelope of the ground response spectra of all the earthquakes expected in a region with a certain probability of occurrence. The ordinate of the design spectrum is a quantity S_a referred to as the *pseudo-acceleration*, which is the maximum relative displacement (with respect to the base) of the oscillator multiplied by the square of its natural frequency. The abscissa is the natural period T, and the damping ratio is usually fixed at 0.05. In this paper we are interested in modifying the accelerogram of a given historic earthquake, such that when its response spectrum is calculated, it is approximately equal to a prescribed design spectrum.

The ground response spectrum of original accelerogram is first calculated at the values of the periods T_j defined by the discrete values of s_j in Eq. (15). Then the ratios γ_j between the values of the target and the calculated spectra are computed:

$$\gamma_j = \frac{[S_a(T_j)]_{\text{target}}}{[S_a(T_j)]_{\text{reconstructed}}} \tag{20}$$

The detail functions $D(s_j, t_k)$, are multiplied by these ratios and a new accelerogram is calculated using Eq. (13). The response spectrum of this updated accelerogram is calculated, a set of new ratios γ_j are computed and the previous detail functions are corrected. The process continues until all the ratios γ_j become sufficiently close to 1 or a pre-established maximum number of iteration is reached.

In order to verify the convergence of the iterative process, a measure of the error is needed. It is proposed to use the Root-Mean-Square of the differences in percent at each of the N periods. At each iteration step the error is calculated as follows:

$$e(\%) = \sqrt{\frac{1}{N}\sum_{j=1}^{N}\left(\frac{S_a(T_j)_{\text{target}} - S_a(T_j)_{\text{reconstructed}}}{S_a(T_j)_{\text{target}}}\right)^2} * 100 \tag{21}$$

Table 1
The scale, dominant frequency and period of selected detail functions

Detail #	j	s_j	ω_j (rad/s)	T_j (s)	f (Hz)
1	−50	0.0131	239.1	0.0263	38.05
10	−41	0.0287	109.6	0.0573	8.33
20	−31	0.0682	46.1	0.1363	7.34

5. Numerical examples

To illustrate the proposed procedure, the records of five earthquakes with widely different characteristics have been selected. It is desired to modify these records so they will be compatible with the ground design spectrum prescribed in the Uniform Building Code (UBC), 1997 Edition (ICBO, 1997) for a seismic zone 3 and soil type S_B (rock). The target spectrum is shown in Fig. 6. The example motions are those registered at: (i) Round Valley, California, November 23, 1984; (ii) Coalinga, California, May 2, 1983; (iii) Loma Prieta, California, October 17, 1989; (iv) Friuli, Italy, September 15, 1976; and (v) Coyote Lake, California, August 6, 1979.

Figs. 5–15 show the spectrum-matching procedure applied to the Round Valley earthquake. The trace of the original round Valley record is shown in Fig. 5. This ground motion has a peak ground acceleration (PGA) equal to 0.088 g and the total duration is approximately 7 s. The response spectrum for a 5% damping ratio of the original record is displayed in Fig. 6.

Fig. 7 shows the coefficients $C(s,p)$ that result from the application of Eq. (2) or rather its discrete version, Eq. (16) to the signal shown in Fig. 5. Note that for the values of the scaling factors greater than about 0.5, the wavelet coefficients decrease significantly. According to Eq. 19 this corresponds to a period $T = (2\pi/\pi)0.5 = 1$ s.

Fig. 8 is similar to Fig. 7, but now the wavelet coefficients $C(s,p)$ are shown in two dimensions and their absolute values are plotted. This is the usual form to graph the coefficients and it is called a Wavelet Map. The lighter colors indicate higher values of the wavelet coefficients. Examining this graph one can observe that the original accelerogram has a dominant component signal around 2–4 s, in a correspondence with a scaling factor of 0.06 (the lightest color in the figure). This value of the scale s is associated to a frequency $\omega = \pi/0.06 = 52.36$ rad/s and a period of 0.12 s. It is interesting to observe that the higher accelerations in the record of Fig. 5 occur between 2 and 4 s. Also the response spectrum in Fig. 6 has its highest peak in the vicinity of a period equal to 0.12 s.

Figs. 9–11 show the detail functions defined in Eq. (17) for the original Round Valley record. Also shown in the same figure is the modulus of the Fourier transform. The original spectrum is shown alongside with the ''smoothed' spectrum. The latter spectrum is obtained by performing a running average of the original spectrum, i.e. calculating each new value as the average of the values at the neighboring points. The smooth spectrum allows one to more clearly appreciate the dominant frequencies. The details functions shown cor-

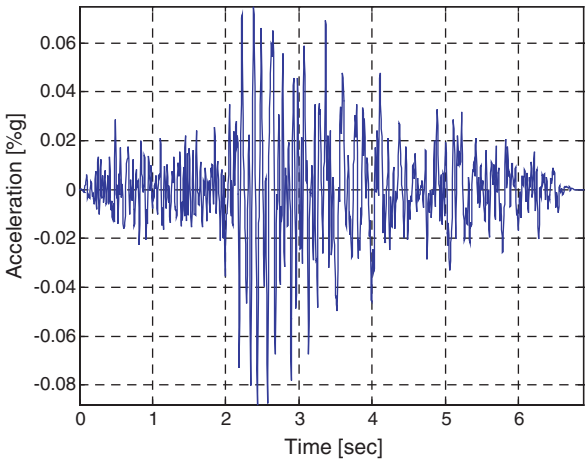

Fig. 5. Original acceleration time history of the Round Valley earthquake.

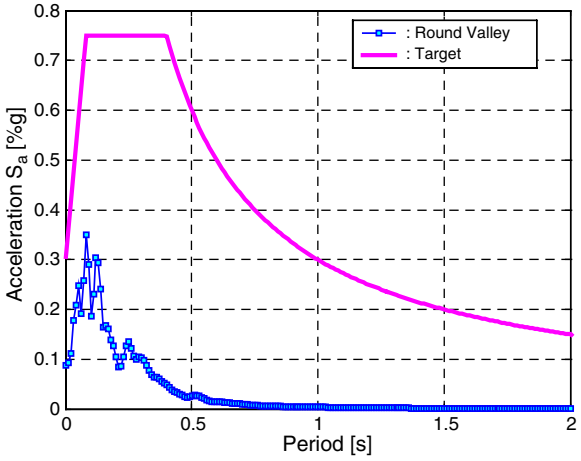

Fig. 6. The UBC-97 zone 3-soil S_B design spectrum and the original response spectrum of the Round Valley record for 5% damping ratio.

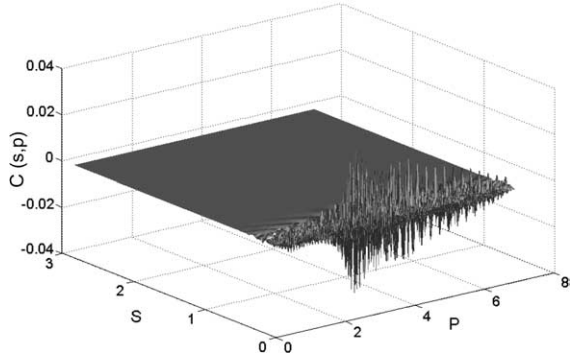

Fig. 7. Coefficients $C(s,p)$ from the Continuous Wavelet Transform for the Round Valley accelerogram.

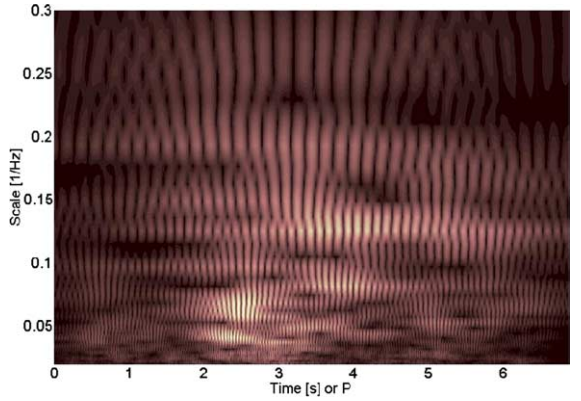

Fig. 8. Top view of the absolute values of the coefficients $C(s,p)$ for the signal of the Round Valley earthquake.

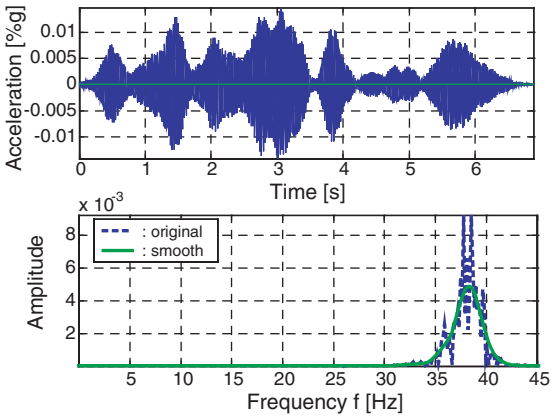

Fig. 9. Detail function # 1($j = -50$) and the magnitude of its Fourier transform with a dominant frequency at 38 Hz.

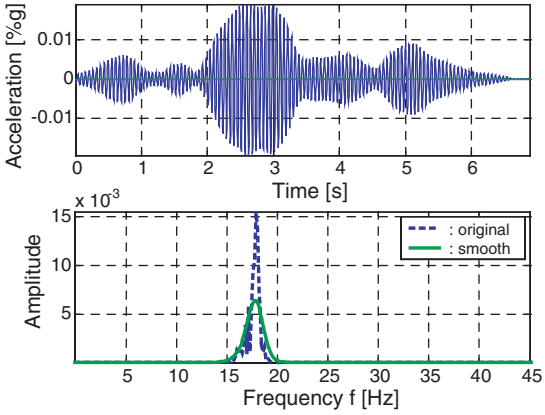

Fig. 10. Detail function # 10 ($j = -41$) and the magnitude of its Fourier transform with a dominant frequency at 17.5 Hz.

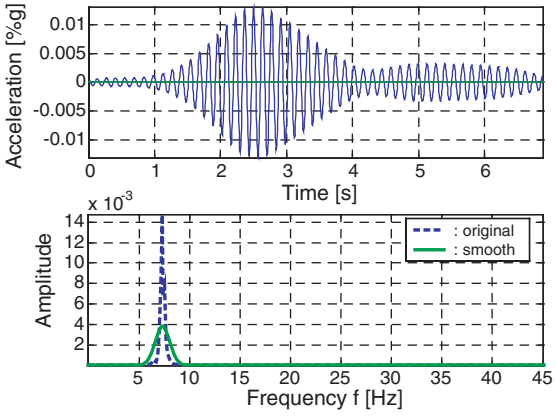

Fig. 11. Detail function # 20 ($j = -31$) and the magnitude of its Fourier transform with a dominant frequency at 7.3 Hz.

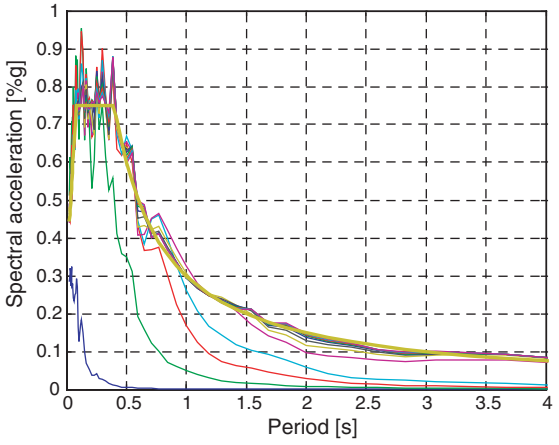

Fig. 12. The target spectrum and the spectra of the modified record of the Round Valley earthquake after each iteration step.

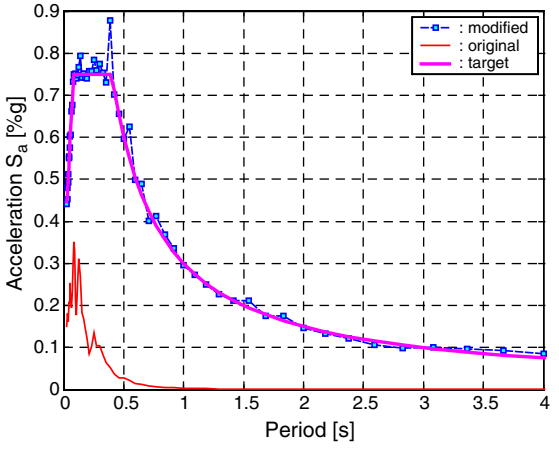

Fig. 13. The target spectrum and the spectra of the original and modified Round Valley record (evaluated at the detail's dominant periods).

respond to the scale parameters listed in Table 1. It can be seen that each detail function has a dominant frequency that coincides with that listed in Table 1.

Fig. 12 shows the results of the matching procedure at each iteration step, i.e. the response spectra of the acceleration time history obtained by adding the detail functions corrected with the factor γ_j defined in Eq. (20). The original spectrum, i.e. the spectrum of the raw signal, is also shown in the figure (the curve near the lower left corner).

For a better visualization the results at the last iteration step are shown separately in Fig. 13. The spectrum is evaluated at the dominant periods of the 63 detail functions with dominant periods ranging from 0.026 to 5.657 s (Fig. 13 only shows the spectrum in the range 0–4 s). To verify the matching at other periods than those of the detail functions, the response spectrum of the modified record evaluated at periods equally spaced at intervals of 0.05 s is shown in Fig. 14.

The final accelerogram compatible with the UBC spectrum is displayed in Fig. 15. This accelerogram should be compared with the original one, shown in Fig. 5. Note that the total duration of the earthquake

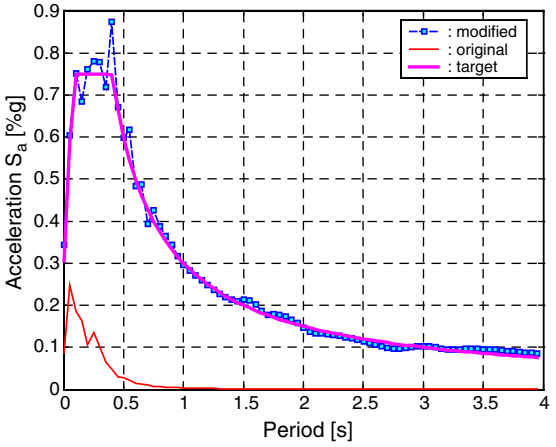

Fig. 14. The target spectrum and the spectra of the original and modified Round Valley record evaluated at equally spaced periods spaced 0.05 s apart.

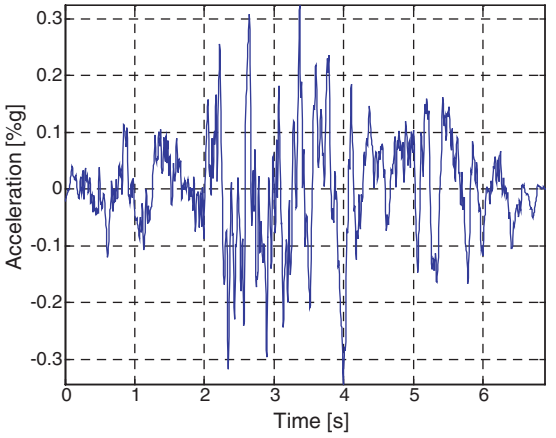

Fig. 15. The modified spectrum-compatible accelerogram of the Round Valley earthquake.

record remains the same (7 s). Note also that some of the high frequency components have been eliminated (or its relative contribution highly diminished). Fig. 16 shows the RMS error defined in Eq. (21) as a function of the iteration steps. As shown in Fig. 16, the error begins at about 60% and rapidly decreases as the iteration process progress. After the sixth cycle the error tend to diminish less quickly. The process was stopped at the eleventh cycle when the RMS error was less than 6%.

The results for the remaining four records, namely the Friuli, Coalinga, Coyote Lake and Loma Prieta earthquakes are shown in Figs. 17–19. Fig. 17 shows the original accelerograms and Fig. 18 displays the corrected time histories. Comparing Figs. 17 and 18, it can be noticed that in the case of the Coyote Lake and Loma Prieta earthquakes, the wavelet-based procedures magnified the relative importance of the component signals with higher frequencies. Interestingly, in the case of the Round Valley earthquake, the opposite was true, i.e. the components with lower frequencies were the ones that were augmented. Fig. 19 shows the matching achieved between the spectra of the four modified earthquake records and the target (UBC Code) spectrum.

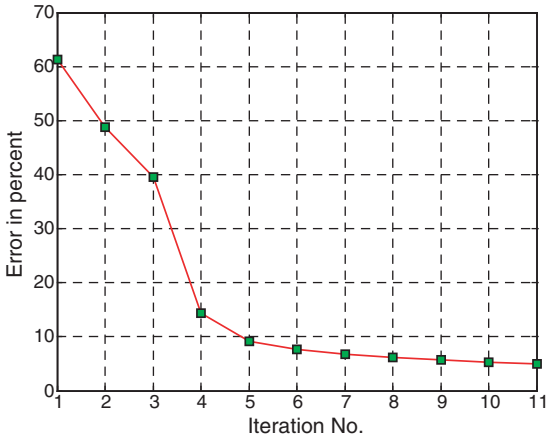

Fig. 16. Variation of RMS error with the iteration step for the Round Valley earthquake.

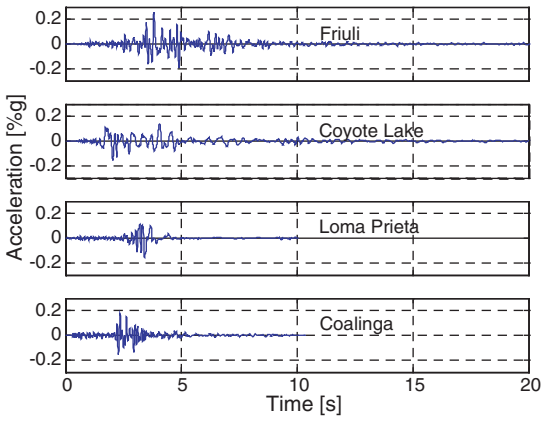

Fig. 17. Original records of the Friuli, Coyote Lake, Loma Prieta and Coalinga earthquakes.

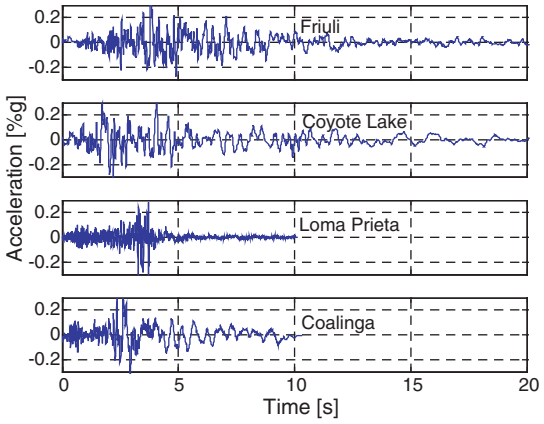

Fig. 18. Modified records of the Friuli, Coyote Lake, Loma Prieta and Coalinga earthquakes.

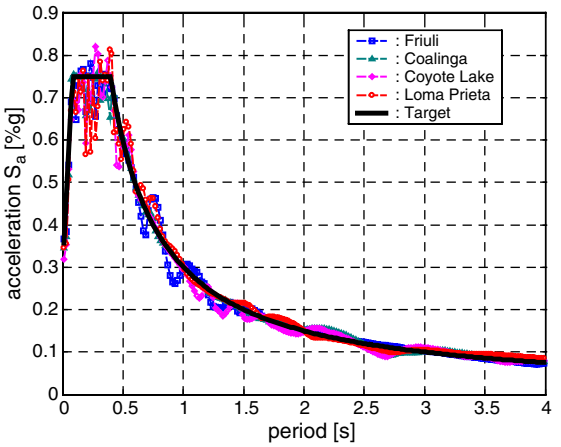

Fig. 19. The target spectrum and the response spectra of the modified records of Friuli, Coalinga, Coyote Lake and Loma Prieta.

6. Conclusions

An application of the wavelet transform to the modification of earthquake records so that they become compatible with a prescribed design spectrum was presented. The original signal is decomposed into detail functions using a new proposed wavelet. The new wavelet is based on the impulse response function of underdamped oscillators. Following an iterative procedure, the detail signals are scaled up or down according to the ratios between the desired design spectrum and the calculated spectrum at a series of discrete periods. It was found that the procedure rapidly and accurately converges to the desired results.

Acknowledgements

This paper is based in the MS thesis of the second author and the work was supported by the Puerto Rico Strong Motion Network under the direction of Dr. José Martínez-Cruzado. This support is gratefully acknowledged.

References

Basu, B., Gupta, V.K., 1998. Seismic response of SDOF systems by wavelet modeling of nonstationary processes. Journal of Engineering Mechanics ASCE 124 (10), 114–1150.

Duval-Destin, M., Muschietti, M.A., Torrésani, B., 1993. Continuous wavelet decompositions, multiresolution, and contrast analysis. SIAM Journal of Mathematical Analysis 24 (3), 739–755.

Grossman, A., Morlet, J., 1984. Decomposition of hardy functions into square integrable wavelets of constant shape. SIAM Journal of Mathematical Analysis 15 (4), 723–736.

International Conference of Building Officials, 1997, Uniform Building Code—1997 Edition, ICBO, Whittier, California.

Mallat, S.G., 1999. A Wavelet Tour of Signal Processing, second ed. Academic press, London, united kingdom.

Misiti, M., Misiti, Y., Oppenheim, G., Poggi, J-M., 2000. Wavelet Toolbox User's Guide. The Math Works Inc., Natick, Massachusetts.

Montejo, L., 2004. Generation and analysis of spectrum-compatible earthquake time-histories using wavelets, MS Thesis, University of Puerto Rico at Mayagüez, Mayagüez, Puerto Rico.

Strang, G., Nguyen, T., 1996. Wavelets and Filter Banks. Wellesley-Cambridge Press, Wellesley, Massachusetts.

Vanmarcke, E.H. and Gasparini, D.A., 1976. Simulated Earthquake Motions Compatible with Prescribed Response Spectra, Report 76-4, Department of Civil Engineering, Massachusetts Institute of Technology, Cambridge, Massachusetts.